Understanding the Crystalline Region Damage Mechanism of XLPE in Water Tree Propagation by Erosion Method

Kangle Li[1], Kai Zhou[2], Hongliang Zhang[1], Hai Jin[1] and Xiaonan Li[1]
[1]College of Electrical Engineering and Information Engineering
Lanzhou University of Technology, Lanzhou, China
[2]College of Electrical Engineering
Sichuan University, Chengdu, China

ABSTRACT

This study investigates the damage characteristics and mechanism of the crystalline regions of cross-linked polyethylene (XLPE) in water tree propagation. XLPE cable samples are subjected to an accelerated water tree aging at a voltage of 7.5 kV/ 400 Hz for 240, 480 and 720 hours. After the water tree aging, the crystalline structural changes of the water tree samples are observed by X-ray diffraction (XRD). In addition, the water tree samples are eroded and the morphologies of the crystalline regions in water tree regions are observed by a scanning electron microscope (SEM). The XRD results show that the crystallinities of the aged samples decrease with aging, especially after 240 hours. The SEM results show that after 240 hours of aging, slip lines and dislocation steps emerge on the fracture surfaces. After 480 hours, microcracks with sizes of several micrometers are observed in the directions of the crystal faces. After 720 hours, conical dislocation pits appear in the samples and there are microvoids at the bottoms of the pits. Based on the XRD and SEM results, it is concluded that the crystalline regions of XLPE are damaged in the water tree aging. At last, the initiation process of the dislocations and the damage characteristics of the crystalline regions in the water tree propagation are discussed.

Index Terms — **XLPE, water tree, crystalline region, damage, dislocations**

1 INTRODUCTION

WATER treeing is one of the main causes for the insulation degradation and life-shortening of cross-linked polyethylene (XLPE) cables [1, 2]. The microstructure of water trees is characterized by interconnected microvoids and nanoscale channels, which is commonly described as 'string pearls' [3]. With the increase in operational years, the microstructure of water trees changes, further leading to the changes of the electric field distributions in water tree regions and water tree propagation behavior [3].

It is generally accepted that water tree propagation can only cause the damage of the amorphous regions of XLPE, and the crystalline regions cannot be damaged [4–6]. However, there is evidence indicating that the crystalline regions of XLPE can also be damaged by water trees. For instance, Fothergill *et al* observed water tree aged samples by small angle X-ray scattering (SAXS) and found that the long-range structure of the crystalline regions (the minimum periodical structure unit) of XLPE was altered [7]. In addition, Tao *et al* observed water tree aged samples by differential scanning calorimetry (DSC) and Raman spectroscopy, and they found that the crystallinities of the water tree aged samples decreased, while the content of non-crystalline regions increased. Based on the experimental results, they considered that the crystalline regions are damaged in the water tree aging. Furthermore, the damaged crystalline regions are transformed to interfacial contents between the amorphous regions and the crystalline regions [8, 9]. However, the existing methods for observing the crystalline structure in water tree samples by indirect detecting methods, there is still no direct evidence of crystalline region damage in water tree aging. In addition, it is hard to know the (possible) damage mechanism of the crystalline regions in water tree aging by indirect detecting methods. Since the crystalline regions of XLPE have a great influence on the mechanical properties of the material [10, 11] and water tree propagation [12–14], the damage phenomenon and mechanism of the crystalline regions in water tree propagation are worth exploring. Thus, whether the crystalline regions of XLPE can be damaged in water tree aging and how the crystalline regions can be damaged, are worth further investigation.

In this study, the microscopic morphologies of the crystalline regions of XLPE in eroded water tree samples are observed by scanning electron microscopy (SEM). Also, the crystallinities

Manuscript received on 1 April 2021, in final form 16 July 2021, accepted 29 November 2021. Corresponding author: K. Li.

DOI: 10.1109/TDEI.2021.009678

of the samples are detected by X-ray diffraction (XRD). Based on the experimental results, the damage characteristics and mechanism of the crystalline regions in water tree aging are revealed.

2 EXPERIMENTAL SETUP

2.1 SAMPLE PREPARATION AND ACCELERATED WATER TREE AGING EXPERIMENT

An 8.7/10 kV XLPE cable (type: $YJLV_{22}$ 3 × 95) was cut into short cable samples with a length of 500 mm. For each sample, the outer semiconductive layer was removed from both ends over 100 mm to ensure sufficient insulation distance, and a 50 mm long conductor was exposed at one end. A copper nose was connected to the exposed conductor for the connection to the high voltage. A 250 mm long part in the middle of the sample was chosen as the accelerated water tree aging area, and two rows of pinhole defects (upper row and lower row) were produced in this area, as shown in Figure 1.

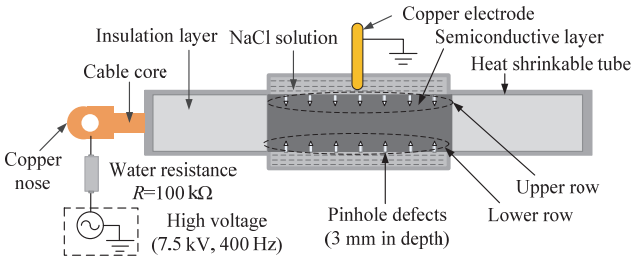

Figure 1. Cable samples and accelerated water tree aging setup.

A syringe needle (diameter: 1 mm, curvature radius of the needle tip: 2.5 ± 0.5 μm) was inserted into the samples in the water tree aging area to produce pinhole defects (the needle was removed to make a pinhole defect). The pinhole defects were 3 mm in depth, and the distance between the pinhole tip and the inner semiconductive layer was 2.5 mm, and the pinholes had the same intervals of 5 mm. Afterwards, a heat-shrinkable tube was placed above the semiconductive layer, and NaCl solution (concentration: 1.8 mol/L) was injected into the tube. Three groups of samples numbered A, B and C were produced by the above method. Each group contained 4 samples and the 4 samples were numbered consecutively as A1–A4, B1–B4 and C1–C4. Before aging, the samples were first stilled for 2 h for wire connection and insulation resistance checking, and then the samples were aged. The aging temperature was room temperature, and the aging time of the three groups of samples were 240 hours, 480 hours, and 720 hours. A voltage of 7.5 kV, 400 Hz was exerted on the samples for the accelerated aging, as shown in Figure 1.

In this study, the frequency of 400 Hz was selected to accelerate water tree propagation. According to previous publications [12] and some repeated experiments, water trees can be steadily initiated at 400 Hz and the water tree shapes at this frequency are similar to those under service conditions.

2.2 MEASUREMENTS

(1) Water tree analysis

To investigate the propagation characteristics of water trees, the aged cable samples numbered 1–2 in each group were sliced for water tree observation. All the pinholes in the samples were sliced. Some 100-μm-thick slices were cut along the pinholes in the direction perpendicular to the sample surface, and then the slices were stained with methylene blue solution at 90℃ for 0.5 h. Afterwards, the slices were observed for water trees through a microscope.

(2) XRD detection

After the water tree aging, the insulation sections (of the samples) containing the pinhole defects (sample 3 in each group) were sliced into plate specimens with dimensions of 10 mm × 10 mm × 2 mm (each plate specimen only contained one pinhole), then the plate specimens were put into a square metal frame and detected by XRD, as illustrated in Figure 2. For each group of samples, three plate specimens were tested. The back side of the specimen (opposite side of the pinhole defects) was detected. In this circumstance, more X-rays can transmit through the water tree regions and more structural information of the crystalline regions can be obtained [15]. In addition, two groups of unaged samples U_1 (without pinhole defects) and U_2 (with pinhole defects) were also detected by XRD for comparative analysis. The type of the XRD apparatus was Ultima IV, and the target in the X-ray tube was Cu. The detection voltage and current were 40 kV and 40 mA, respectively, and the detection angle was in the range of 2–90°. The scanning area of the X-ray on the sample surface ranged from 10 mm × 10 mm (2°) to 10 mm × 3.08 mm (90°). The incident energy of the X-ray was about 3.2 W, and the penetration depth of the X-ray was about 12 mm. By changing the incident angle of the X-ray, the whole water tree area can be scanned and the crystalline region information in the water tree area can be obtained.

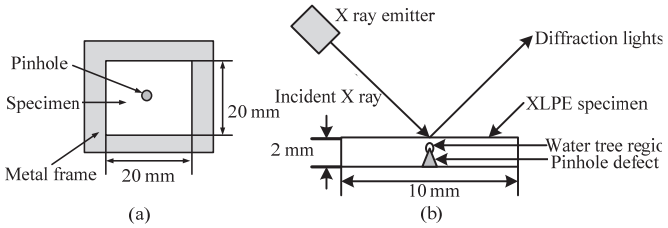

Figure 2. XRD detection principle of the plate specimen: (a) specimen frame and (b) detection method.

(3) Erosion and SEM observation

Figure 3 shows the typical dislocation shapes (such as dislocation pits and steps) in metals observed by erosion method. It is worth noting that the structures of the crystals of XLPE and metals are similar (ordered arrangements of atoms or structural units), so the damage characteristics and regularities of the two substances can be similar. By comparing the damage morphologies of the crystalline regions of XLPE in water tree regions with those of the metals, the damage characteristics of the crystalline regions of XLPE in water tree aging can be obtained.

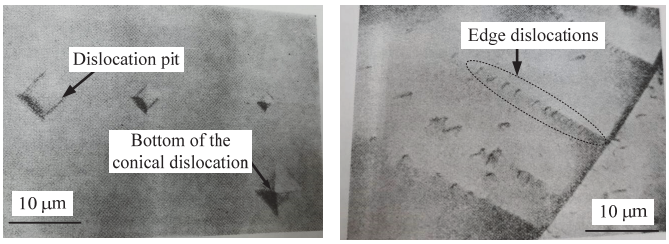

Figure 3. Typical dislocation shapes in eroded metals: (a) dislocation pits (in LiF [16]) and (b) edge dislocations (in stainless steel [17]).

Among the direct methods of observing dislocations in crystals, the erosion method is the simplest and the most widely used [13]. The energy in the dislocation (crystal distortion) parts is higher than the ordered parts. For this reason, after eroded by suitable erodent and erosion time, the outcrops of the dislocations on the surface of the crystals (the intersections between the dislocations and the crystal surface) are easiest to be eroded and etch steps or pits can be formed. The most evident appearance feature of dislocations is conical pits with sharp bottoms [18], as shown in Figure 3a. In addition, orderly arranged edge dislocations are also typical dislocation (movement) appearances [17], as shown in Figure 3b.

The aged samples (numbered 4 in each group) were observed by SEM. First the samples were cut into shorter sample sections containing the pinhole defects and divided into two smaller groups (one group contains the pinholes in the upper side and the other group contains the pinholes in the lower side). Afterwards, all the sample sections were broken at the pinholes at about –200 ℃. The broken sections in the upper side of the samples were directly observed by SEM, and the broken sections in the lower side of the samples were first immersed in the etchant of potassium permanganate and concentrated sulfuric acid (the mass ratio of the two components is 1: 20) at room temperature for 72 h, and then they were observed by SEM.

According to repeated erosion experiments on water tree aged samples aged for 720 hours, if the erosion time is too short (such as 24 h), the dislocations in the samples cannot be observed (Figure 4a). However, if the erosion time is too long (such as 240 h), the dislocations can be damaged. As shown in Figure 4b, there are microcracks on the inclined plane and bottom of the dislocation pit and the pit shape becomes blurry. Only eroded for suitable time (72 h), the dislocations can be clearly observed, as shown in Figures 4c and 4d. In the figures, the inclined planes and the conical shape of the dislocation pit are clear. Eventually the erosion time of water tree aged samples is determined to be 72 h. It is worth noting that in SEM observation, the shade of color can reflect the depth of the surface. The darker the color, the lower the surface. From Figures 4b–4d, the colors of the pits become deeper from the edges to the inner parts, therefore, it can be judged that the pits are V-shaped grooves with two inclined planes.

After erosion, the eroded samples were cleaned by dilute hydrochloric acid for 15 min and observed by SEM. In addition, two other groups of unaged samples were eroded for 72 h and 240 h for comparative analysis with water tree samples and observation of crystalline region morphologies. The type of the SEM instrument was JSM-7500F, and it had a resolution of 1.4 nm under a voltage of 1 kV. The experimental setup of the water tree samples is shown in Table 1.

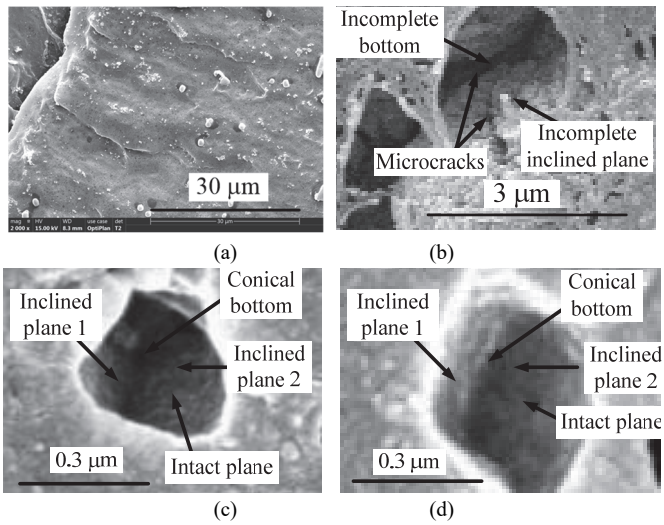

Figure 4. Dislocation pit morphologies in water tree samples aged for 720 hours and eroded for different times: (a) eroded for 24 h, (b) eroded for 240 h and (c and d) eroded for 72 h.

Table 1. Experimental setup of the samples.

Group number (sample number)	Aging time/hours	Observations			
		Water tree	XRD	SEM	
				Uneroded	Eroded
U_1 (no pinholes)	0	No	Yes	No	No
U_2 (pinholes)	0	No	Yes	Yes	Yes
Group A (1–4#)	240	Yes (1–2#)	Yes (3#)	Yes (4#US)	Yes (4#LS)
Group B (1–4#)	480	Yes (1–2#)	Yes (3#)	Yes (4#US)	Yes (4#LS)
Group C (1–4#)	720	Yes (1–2#)	Yes (3#)	Yes (4#US)	Yes (4#LS)

Note: US the upper row of the pinholes, LS the lower row of the pinholes.

3 EXPERIMENTAL RESULTS

3.1 WATER TREE ANALYSIS

The typical water tree morphologies in the water tree aged samples are shown in Figure 5. In the water tree aging, since the water filled pinholes are taken as the high voltage electrode, it is hard for charges to inject into the XLPE insulation from the pinholes [6]. In addition, before aging, the samples are stilled for 2 hours to connect wires and check the insulation resistances of the samples. In this period, the NaCl solution can diffuse into the microcracks induced by the insertion of the needles, and partial discharges can be inhibited [6]. For this reason, electrical trees will not be initiated in the water tree regions.

The water tree length distributions and propagation rates of water trees in the three groups of samples are shown in Figure 6. The water tree length refers to the lengths of the longest water tree branches. From Figure 6, the propagation rate of water trees decreases significantly to 0.17 μm/h after 720 hours of aging.

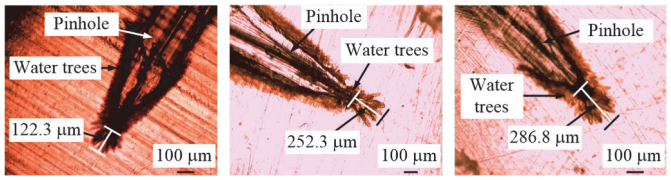

Figure 5. Water tree morphologies in the three groups of samples: (a) 240 hours, (b) 480 hours and (c) 720 hours.

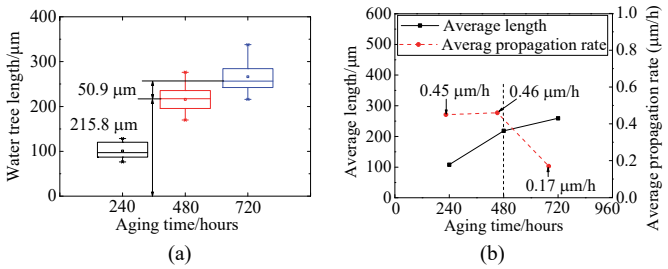

Figure 6. Water tree length distributions and propagation rates in the three groups of samples: (a) water tree length distributions and (b) propagation rates.

3.2 XRD DETECTION PRINCIPLE OF DISLOCATIONS

(1) Crystal structures of XLPE

Crystals are formed by the periodical ordered arrangements of structural motifs in the space, and crystalline cells are the basic structural units of crystals. XLPE crystals are orthorhombic and the lengths of the three crystalline axes (of the crystalline cells) are: a = 0.74 nm, b = 0.49 nm, c = 0.25 nm, as shown in Figure 7a.

Because of ordered arrangements, various families of parallel crystal faces are formed, and a certain family of the crystal faces is commonly defined as crystal face index of (hkl), where h, k, l are the reciprocals of the intercepts of the crystal faces in the crystalline axes [15]. As shown in Figure 7a, the intercepts of the crystal face ABCD in x, y, z axes are 1, 1, ∞, so the crystal face index of the crystal faces is (110). In addition, according to the magnitude of the crystal face distances, the crystal faces can be grouped as the main crystal face, the second crystal face et al. The main crystal face (with the largest crystal face distance) of XLPE is (110), followed by (200) and (020). The larger the distance between the crystal faces, the weaker the acting forces and the smaller the shear strength of the crystal faces. For this reason, the shear strength of (110) (crystal face) is the smallest and is easiest to initiate dislocations, followed by (200) and (020). The angles between the three crystal faces of (110), (200) and (020) are shown in Figure 7b.

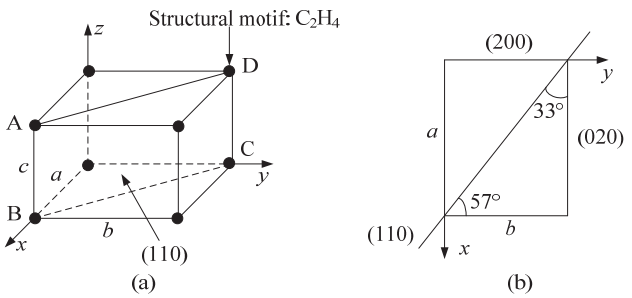

Figure 7. Crystal structure of XLPE: (a) crystal face index and (b) angles between crystal faces.

(2) Concept of dislocations

Dislocations are crystal defects where the arrangements of the atoms deviate from equilibrium positions [18]. There are two basic types of dislocations: screw dislocation and edge dislocation. As shown in Figure 8a, suppose a crystal is cut along y direction on plane π (parallel to xoy plane) and the two cross sections (upper part and lower part) move relatively and form a dislocation under a shear stress τ, then the boundary between the ordered and misaligned parts is defined as the dislocation line. In addition, the vector of the direction and magnitude of the relative displacement is generally denoted as b, namely the Burgers vector, the direction of which is in accordance with τ.

According to the relative direction of the Burgers vector and dislocation line, the dislocations can be divided into two types. If the Burgers vector is perpendicular to the dislocation line, the dislocation is an edge one, while if the Burgers vector is parallel to the dislocation line, then the dislocation is a screw one. The basic characteristic of the edge dislocation is that there is one more piece of semiatomic plane above plane π, like ABCD in Figure 8b, while the basic characteristic of the screw dislocation is the relative movement of the two cross sections for b, as shown in Figure 8c [18].

The basic movement form of dislocations is slip. When the dislocation slips out of the crystals, a dislocation step is formed along the direction of the Burgers vector, as shown in Figures 8d and 8e. In addition, there is cross slip of screw dislocations, namely successive slips along different parallel crystal faces. The cross slip can form mansard slip tracks, such as ABF in Figure 8f, which is formed by the slip on π (under τ_2) and then on π' (under τ_3).

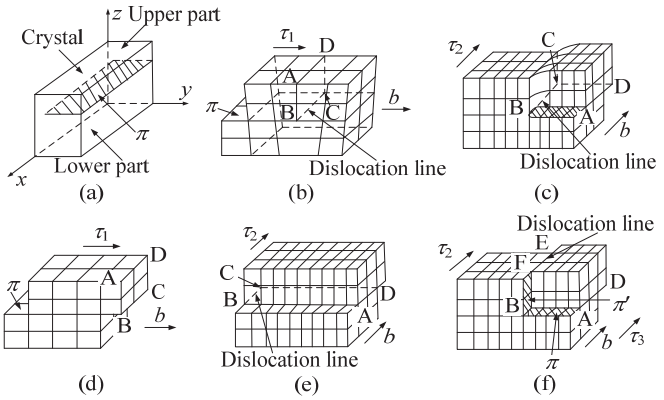

Figure 8. Different dislocation types and their movements: (a) ordered crystal, (b) edge dislocation, (c) screw dislocation, (d) slip of edge dislocation, (e) slip of screw dislocation and (f) cross slip of screw dislocation.

(3) XRD detection principle of dislocations

According to the Bragg diffraction condition [15], the interference condition of the emergent rays is:

$$\Delta = 2d_{hkl}\sin\theta_{hkl} = n\lambda, n = 1, 2, 3, \ldots \quad (1)$$

where Δ is the optical path difference of the emergent rays, d_{hkl} the distances between crystal faces, θ_{hkl} the incident angle when interference happens, and λ the wavelength of X-ray, and there

is one-to-one correspondence between d_{hkl} and θ_{hkl}. For a certain family of crystal faces, d_{hkl} is a constant.

In XRD analysis, the half peak width (*FWHM*) is generally used to evaluate the distortion degree of the crystals [15], and it is defined as the angle range corresponding to the half peak intensity. The larger the *FWHM*, the more the dislocations and the larger the distortions.

3.3 XRD DETECTION RESULTS

The XRD detection results of the unaged samples (with and without pinholes) and the water tree aged samples are shown in Figure 9, where 2θ represents the diffraction angle. The diffraction angles of the samples are in the range of 10–30° [15], including the amorphous peak (19.5°), the crystalline region peak of (110) (strongest peak, at 21.2°) and the crystalline region peak of (200) (sub strong peak, at 23.5°). Based on the detection results, the half peak widths of the two strong peaks and the average crystallinities of the samples are calculated, and the calculation results are shown in Table 2 [19].

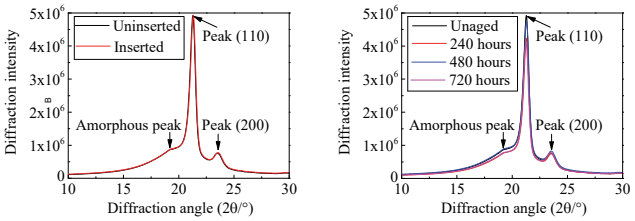

(a) (b)

Figure 9. XRD diffraction curves of the samples: (a) unaged samples and (b) water tree samples.

Table 2. XRD diffraction data of the samples.

Group number	Aging time/hours	*FWHM* (110)	*FWHM* (200)	Average crystallinity/%
U_1 (no pinholes)	0	0.6311	0.6232	44.5
	0	0.6313	0.6235	
U_2 (pinholes)	0	0.6314	0.6236	44.5
	0	0.6311	0.6232	
	240	0.6335	0.6256	
Group A	240	0.6342	0.6266	44.2
	240	0.6352	0.6278	
	480	0.6382	0.6318	
Group B	480	0.6389	0.6333	43.7
	480	0.6383	0.6320	
	720	0.6502	0.6604	
Group C	720	0.6506	0.6610	42.2
	720	0.6511	0.6625	

From Table 2, compared with the unaged samples without pinholes, the *FWHM* of the two strong peaks of the unaged samples with pinholes increase by 0.1% and 0.3%, and they are much smaller than the water tree aged samples (above 2%). Therefore, the widening of the peak (increase in *FWHM*) caused by the pinhole defects does not influence the judge and analysis of the crystal distortions caused by water trees.

The diffraction parameters of the water tree aged samples change significantly compared with unaged samples:

1) *FWHM*: the half peak widths of peaks (110) and (200) of water tree aged samples are much higher than unaged samples and increase with aging. For instance, the *FWHM* of peak (110) increases to 0.6382 after 480 hours of aging, which increases by 1.09% compared with unaged samples.

2) Crystallinity: the crystallinity of the water tree aged samples decreases, especially after 240 hours. For instance, the average crystallinity of the samples aged for 240 hours decreases by 0.67%, while between 240 and 480 hours of aging, the average crystallinity of the samples decreases by 1.13%. From the above results, the crystalline regions of XLPE are damaged in water tree aging, especially after 240 hours.

3.4 SEM OBSERVATIONS

The morphologies of the spherulites of XLPE insulation (erosion time: 240 h) are shown in Figure 10a. The diameters of the spherulites are about 5 μm. In addition, there are gaps between the spherulites, which are eroded amorphous regions. The SEM observation results of the eroded unaged samples (erosion time: 72 h) are shown in Figure 10b. The surface of the unaged samples is smooth.

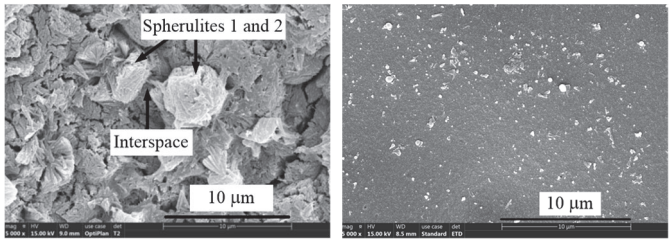

(a) (b)

Figure 10. The morphologies of the crystalline regions of XLPE and unaged samples: (a) crystalline regions of XLPE, eroded for 240 h and (b) eroded unaged samples, eroded for 72 h.

The SEM observation results of the uneroded water tree aged samples are shown in Figure 11. There are microvoids in the samples, and no micron-size channels (typical microstructural characteristics of electrical trees [20]) are observed. The results show that the voids are caused by water tree aging [4]. In addition, since the crystalline region damage cannot be

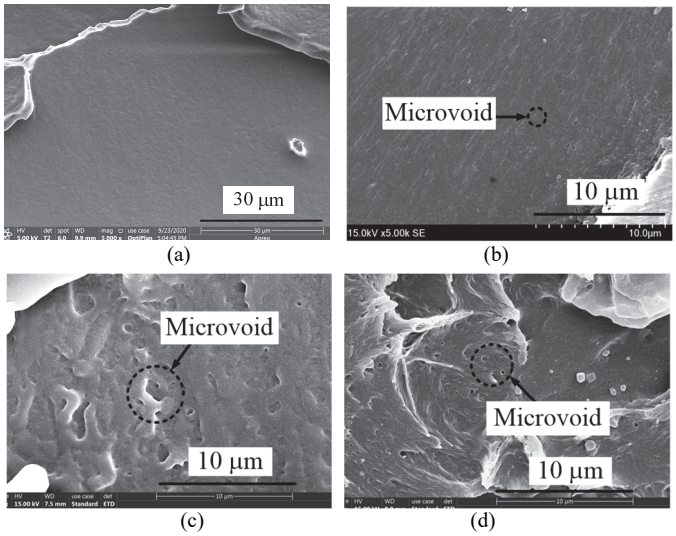

(a) (b) (c) (d)

Figure 11. Microscopic morphologies in unaged samples and water tree samples without erosion: (a) unaged, (b) aged for 240 hours, (c) aged for 480 hours and (d) aged for 720 hours.

distinguished without erosion, Figure 11 mainly reflects the microscopic morphologies of the amorphous regions.

The SEM observation results of the eroded water tree aged samples are shown in Figure 12. In Figure 12, the long dash lines denote the directions of the crystal faces, and the short dash lines denote the directions of the slipping lines, the extension directions of dislocations and microcracks. (110), (200) and (020) are crystal face indexes, and the sequence of them are determined according to the directions of the slip lines and the dislocations. From Figure 12, there are typical dislocation morphologies, such as slip lines and sharp bottomed pits (Figure 12f) in the eroded samples, and the typical dislocation morphologies are repeatedly observed. The above results prove that the defects in eroded water tree aged samples are dislocations in the crystalline regions.

From Figure 11, the microscopic morphologies of the amorphous regions are characterized by the increase of the size and density of the round microvoids. Since the amorphous regions are isotropic, the amorphous region damage can also be isotropic and round voids are formed.

By comparison, the microscopic morphologies of the crystalline regions can change with aging. As shown in Figures 12a and 12b, after 240 hours of aging, slender screw dislocation slip lines, screw and edge dislocation steps are observed in the directions of the three crystal faces of (110), (200) and (020), and the lengths of the slip lines reach 100 μm. In addition, there are cross slip tracks of screw dislocations, and the angle between the adjacent two track lines is about 130°, which is close to the angle between the crystal faces of (110) and (200), as shown in Figure 12b. After 480 hours of aging, microcracks appear in the directions of the crystal faces. For instance, microcracks 1 and 2 are along the directions of crystal face of (020), and microcrack 3 is along the direction of crystal face of (110) (Figure 12c). The length of microcrack 1 reaches 7.5 μm. In addition, the appearance of the cross slip tracks of screw dislocations become clearer, and the angles between different lines of the tracks are about 130° and 150°, which are close to the angles between the three crystal faces, as shown in Figure 12d. After 720 hours of aging, the lengths of the microcracks along the crystal directions increase and reach about 100 μm, as shown in Figure 12e. Moreover, large numbers of different shaped conical dislocation pits (such as V shaped groove and L shaped, U shaped pits) appear in the samples, and there are microvoids at the bottom of the pits, as shown in Figure 12f. Since the crystalline regions are anisotropic, the damage of the regions can also be anisotropic, and there can be different damage morphologies in the crystalline regions in different aging periods.

It is worth noting that the damage morphologies of the crystalline regions of different specimens in the same group of samples can be different. For instance, in the samples aged for 240 hours, there are slip lines and dislocation steps in specimen 1 (Figure 12a), while there are only dislocation steps in specimen 2 (Figure 12b). The cause for the different damage morphologies in the same group of samples will be discussed in detail in Section 4.2.

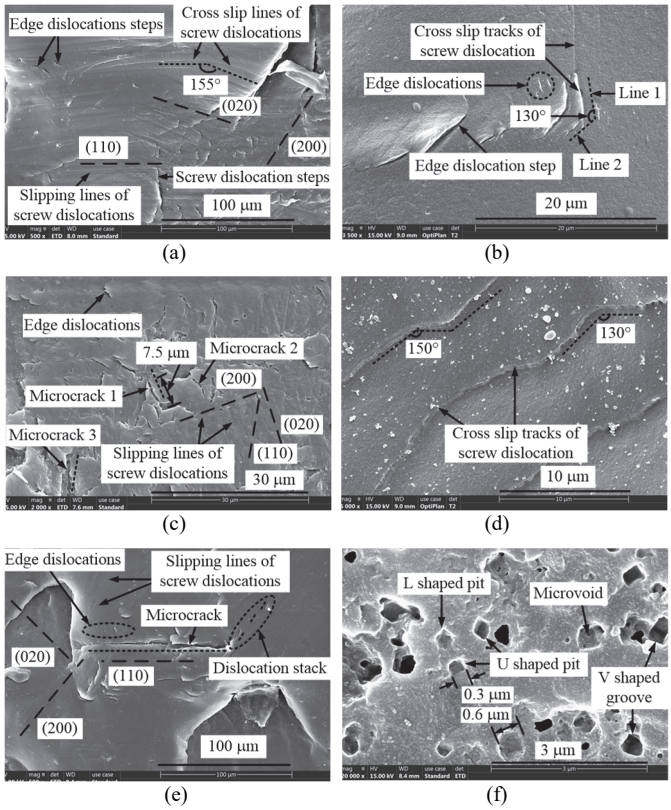

Figure 12. Microscopic morphologies of water tree regions in eroded samples: (a and b) aged for 240 hours, (c and d) aged for 480 hours and (e and f) aged for 720 hours.

4 DISCUSSION

4.1 DISLOCATION INITIATION OF THE CRYSTALLINE REGIONS IN WATER TREE AGING

XLPE is a semi-crystalline polymer which is composed of the amorphous regions and the crystalline regions. The molecular chains in the amorphous regions are in random coil, while the molecular chains in the crystalline regions are orderly arranged to form crystal wafers and crystals. The cohesive energy density and mechanical strength of the amorphous regions are much lower than the crystalline regions, so the amorphous regions can be damaged first in the water tree aging.

In the initial stage of the water tree aging, water first diffuses into the free volumes of the amorphous regions of XLPE to form isolated water filled cavities. Since the electric field can be strong at the pinhole tip, water can reach saturation in the material around the pinhole tip in a short time. The water filled cavities can exert Maxwell forces on the molecular chains in the amorphous regions, and the molecular chains can deform and fracture to initiate microcracks and microvoids. When the microvoids are interconnected by the microcracks, water tree branches can be formed [2], as shown in Figure 13a. It is worth noting that the saturation of water usually takes some time, so water tree does not grow from the very beginning of aging but after some time.

With the increase in aging time, the microvoids in the amorphous regions gradually develop to the crystalline regions and exert Maxwell forces on the crystalline regions, as shown

in Figure 13b. As a result, the crystalline regions deform and dislocations can be initiated, as shown in Figure 13c. These dislocations and the inherent dislocations become the initial dislocation sources in the crystalline regions.

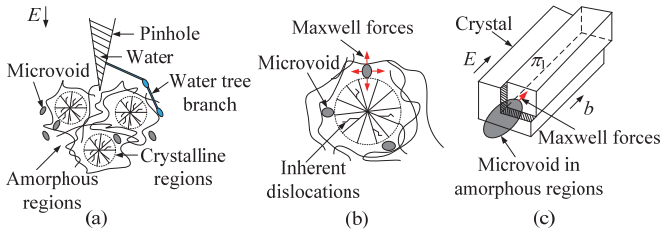

Figure 13. Initiation process of dislocations: (a) microvoid formation in the amorphous regions, (b) microvoid enlargement in the amorphous regions and (c) initiation of dislocations in crystals.

4.2 DAMAGE PROCESS OF THE CRYSTALLINE REGIONS OF XLPE IN WATER TREE AGING

According to the Peierls-Nabarro model of the dislocation movement [18], the slip resistance (or driving force) of the dislocation movement τ_p can be expressed as:

$$\tau_p = \frac{2G}{1-\upsilon}\exp\left(-\frac{2\pi}{1-\upsilon}\right)\cdot\frac{a}{b} \tag{3}$$

where G is the shearing strength of the crystalline regions (1.3–4 MPa), υ the Poisson's ratio (0.4), a and b the lengths of the crystal axes. Based on Equation (3), the slip resistance of the dislocation movement in the crystal faces of (110) of XLPE is about 0.006 MPa.

Based on previous simulations, the Maxwell forces around the water tree voids are about 0.02–0.06 MPa [6], which can be higher than the driving forces of the dislocation movement. For this reason, the dislocations are easy to move in the crystalline regions and can proliferate under the Maxwell forces.

The deformation and damage of the crystals are mainly caused by the movement of dislocations. Due to different dislocation types and movement directions, the proliferation of the dislocations and the damage of the crystalline regions can be much more complex than the damage of the amorphous regions. As previously mentioned, the crystalline regions are anisotropic, and the shear strengths of different crystal faces are different. Therefore, dislocations can be first initiated and proliferate in the crystal face of (110), and then in the crystal faces of (200) and (020).

Before 240 hours of aging, edge and screw dislocations are initiated on crystal faces of (110), (200) and (020). Since the water tree void density is small in the amorphous regions, the dislocation density is also small, and the dislocations can slip for long distances in the crystals. Since the Burgers vector of an edge dislocation is parallel to its movement direction, when the edge dislocation slips across the crystals, the rest of the crystal parts are intact. When the edge dislocation slips out of the crystals, a dislocation step can be formed, and the length of the step is equal to the dislocation line, as shown in Figure 14a.

By comparison, the Burgers vector of a screw dislocation is perpendicular to its movement direction, when the screw dislocation slips across the crystals, the crystal faces become spiral surfaces. Since the atoms in the dislocation lines deviate away from the equilibrium positions, when the crystals are eroded, slip lines can be formed in the spiral surface parts, and the lengths of the slip lines are equal to the lengths of slip distances. When the screw dislocation slips out of the crystals, steps can be formed out of the crystal, and the lengths of the steps are equal to the lengths of the slip distances, as shown in Figure 14b. For this reason, when screw dislocations slip for a long distance, long slip lines or steps can be formed within or out of the crystals. Due to the different relative directions between the screw dislocations and the fracture surfaces, different damage morphologies of the crystalline regions can be observed. As shown in Figure 14b, when the fracture surface is parallel to the plane of yoz, slip lines can be observed. However, when the fracture surface is parallel to the plane of xoz, dislocation steps can be observed. Combining with the different damage morphologies in the samples with the same aging time, the damage characteristics of the crystalline region of XLPE can be more clearly determined.

In addition, the screw dislocation can experience cross slip and form cross slip lines (steps), as shown in Figure 14c. Since the screw dislocations slip on the crystal faces, the directions of the slip lines (steps) and the angles between adjacent cross slip lines are in accordance with the directions of the crystal faces or the angles between adjacent crystal faces.

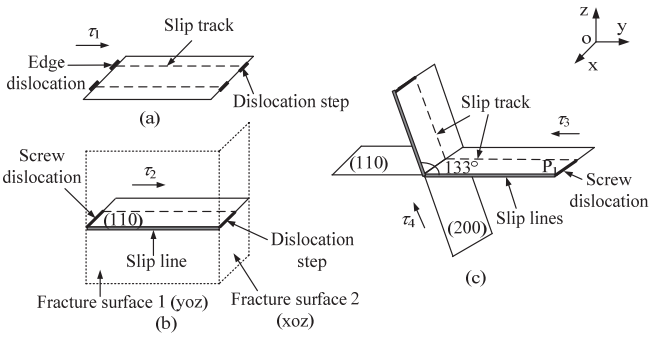

Figure 14. Slip morphologies of edge and screw dislocations. (a) Slip of edge dislocations, (b) slip of screw dislocations and (c) cross slip of screw dislocations.

After 480 hours of aging, the density of the water tree void increases and more dislocations are initiated in different crystal faces. Dislocations in different crystal faces can encounter and intersect with each other. As shown in Figure 15a, suppose there are two edge dislocations AB and XY in the crystal faces of (200) and (020), and they are formed under the shear stresses of τ_1 and τ_2 (τ_{p1} and τ_{p2} are slip resistances, the same below), the Burgers vectors of the two dislocations are b_1 and b_2 and they are perpendicular to each other. When the two dislocations intersect, an edge type jog PP' can form on AB, as shown in Figure 15b [16]. Afterwards the dislocation lines AP and P'B on the two sides of PP' continue to move on the crystal face of (200), while PP' moves on the crystal face of (020). Since the acting force between the crystal faces of (020) is larger than that in the crystal faces of (200), the slip resistance of PP' can be larger than the slip resistances of AP and P'B. In other words, the jog can hinder the movement of the dislocations. With more

intersections of dislocations, the jog PP' enlarges, correspondingly the slip resistance increases. When the external shear force cannot surmount the slip resistance, subsequent dislocations initiated on the crystal faces of (200) can be stacked at PP', as shown in Figure 15c, where ⊥ denotes the edge dislocations.

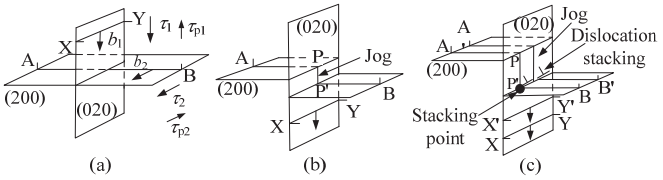

Figure 15. Intersection and stacking of dislocations: (a) dislocation intersection, (b) jog formation and (c) stacking of dislocations.

As shown in Figure 16a, suppose the edge dislocations are stacked at PP', and the length of the dislocation line is L. The shear stress at r (near P) is (r is much less than L) [18]:

$$\tau \approx \tau_0[1+(L/r)^{1/2}] \tag{4}$$

where τ_0 is the magnitude of the shear stress. From the equation it can be known that dislocation stacking can result in stress concentration. For instance, if the length of the dislocation line on the crystal face (200) is 100 nm and r is 2 nm, then τ is about $8\,\tau_0$. If τ_0 is 0.01 MPa, when the number of the stacked dislocations reaches 50, the position where dislocations are stacked can initiate microcracks (suppose the shear strength of the crystals is 4 MPa), as shown in Figure 16b. In addition, since the dislocations are stacked along the directions of the crystal faces, the microcrack can extend along the directions of the crystal faces, as shown in Figure 16b.

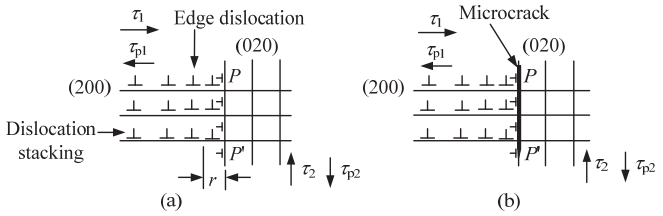

Figure 16. Stacking of dislocations and initiation of microcracks. (a) Stacking of dislocations and (b) initiation of microcracks.

After 720 hours of aging, more dislocations can intersect and be stacked, at this time different types of dislocations on different crystal faces can proliferate to form different shaped dislocation pits. The V shaped dislocation groove is formed by the proliferation of edge dislocations in different crystal faces. As shown in Figure 17a, suppose there are two edge dislocations on crystal faces P_1 and P_2 (their dislocation lines are perpendicular to the paper), and the Burgers vectors of the two dislocations are b_1 and b_2, respectively. Under the shear stresses of τ_1 and τ_2, the upper part of P_1 slips towards the lower left, while the upper part of P_2 slips towards the lower right (Figure 17b), eventually V shaped dislocation grooves are formed, as shown in Figure 17c.

The L shaped dislocation pits observed in the eroded samples (aged for 720 hours, Figure 12f) are formed by the polar axis

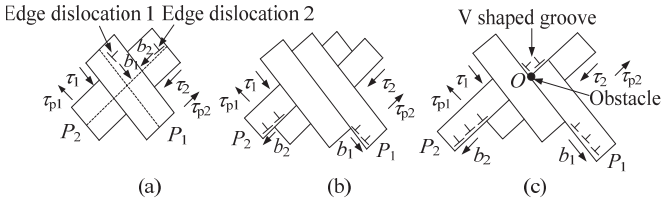

Figure 17. Formation of V shaped groove: (a) encounter of edge dislocations, (b) slip of crystal faces and (c) formation of V shaped groove.

mechanism, namely the rotation of an edge dislocation (formed under τ_1) around spiral surfaces caused by a screw dislocation (formed under τ_2), as shown in Figure 18a. In the figure, PP' is the dislocation line of the screw dislocation, namely, the polar axis, π_1, π_2 and π_3 et al are spiral surfaces. In addition, CDE is an L shaped edge dislocation (Frank-Read source [18]), and point D is the fixed point. When CD rotates around D on π_1 for one circle, the crystal parts above π_1 move b_1 to the back of the crystal. In the meantime, CD drops down to π_2 [18]. When CD rotates n circles, the crystals can experience substantial displacements and a pit can form in the sliding parts, as shown in Figure 18b. When water diffuses into the pit, electric field can distort at the pit, so τ_1 increases, and larger displacements occur. As a result, the length of the dislocation line increases. With the further rotations of the edge dislocations, the dislocation pit not only deepens, but the dislocation line becomes longer as well, eventually conical dislocation pits are formed, as shown in Figure 18c. Moreover, since the electric field distortion is larger at the bottom of the dislocation pit, microvoids can be initiated at the bottom of the pit [21]. Similarly, U shaped dislocation pits are formed by the rotations of U shaped edge dislocations around screw dislocations.

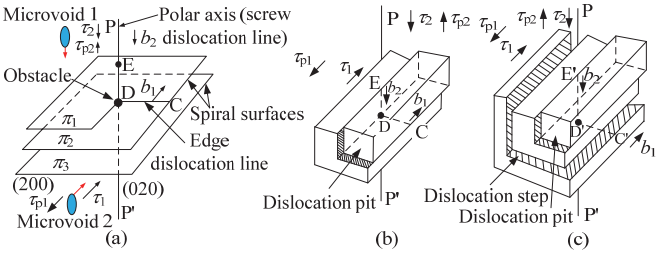

Figure 18. Formation of L shaped dislocation pit: (a) encounter of an edge dislocation and a screw dislocation and (b andc) formation process of dislocation pit.

From the above analysis, the dislocations proliferate to form slip lines, dislocation pits and microcracks and microvoids are initiated. Before 240 hours of aging, only slip lines are formed but the crystalline regions are not damaged (or the damage extent is low), so the crystallinities of the samples do not decrease much. However, after 240 hours of aging, microcracks and microvoids are initiated in the crystalline regions, so the crystallinities of the samples decrease significantly.

5 CONCLUSIONS

(1) The crystalline regions of XLPE can be damaged in the propagation of water trees. After 240 hours of aging, slip lines

and steps are formed in the samples. After 480 hours, microcracks are initiated in the crystal faces of (110), (200) and (020). After 720 hours of aging, V shaped groove and L shaped, U shaped dislocation pits are formed. Moreover, there are microvoids at the bottoms of the dislocation pits.

(2) The initiations of the initial dislocations in the crystalline regions of XLPE originate from the deformation of the crystals caused by the water filled microvoids in the amorphous regions. When the deformation stress exceeds the shear strength of the crystal faces, dislocations are initiated.

(3) The damage of the crystalline regions originates from the intersection and proliferation of different dislocations. In the initial aging period, the dislocations move for long distances in the crystals to form slender slip lines and dislocation steps. With the increase in the dislocation density, dislocations in different crystal faces intersect with each and result in the stacking of dislocations and initiation of microcracks. When the dislocation density is high, different dislocations proliferate to form dislocation pits and microvoids can be initiated at their bottoms.

ACKNOWLEDGMENT

The authors thank the National Science Foundation of China under Projects No. 51607082 and 51877142 for providing financial support for this research. We also appreciate Hui Wang from the Analytical & Testing Center of Sichuan University for her help with SEM characterization.

REFERENCES

[1] E. F. Steennis and F. H. Kreuger, "Water treeing in polyethylene cables," IEEE Trans. Electr. Insul., vol. 35, no. 5, pp. 989–1028, 1990.
[2] R. Ross, "Inception and propagation mechanisms of water treeing," IEEE Trans. Dielectr. Electr. Insul., vol. 5, no. 5, pp. 660–680, 1998.
[3] J. L. Chen and J. C. Filippini, "The morphology and behavior of the water tree," IEEE Trans. Electr. Insul., vol. 28, no. 2, pp. 271–286, 1993.
[4] L. A. Dissado, S. V. Wolfe and J. C. Fothergill, "A study of the factors influencing water tree growth," IEEE Trans. Electr. Insul., vol. 18, no. 6, pp. 565–585, 1983.
[5] J. P. Crine and J. A. Jow, "A water treeing model," IEEE Trans. Dielectr. Electr. Insul., vol. 12, no. 4, pp. 801–808, 2005.
[6] K. Zhou *et al*, "A possible water tree initiation mechanism for service-aged XLPE cables: conversion of electrical tree to water tree," IEEE Trans. Dielectr. Electr. Insul., vol. 23, no. 3, pp. 1854–1861, 2016.
[7] J. C. Fothergill *et al*, "Electrical, microstructural, physical and chemical characterization of HV XLPE cable peelings for an electrical ageing diagnostic database," IEEE Trans. Dielectr. Electr. Insul., vol. 10, no. 3, pp. 514–527, 2003.
[8] X. Tao *et al*, "Trap characteristic and potential trap model of water trees in XLPE," *Annu. Rep. Conf. Electr. Insul. Dielectr. Phenom. (CEIDP),* 2018, pp. 378–381.
[9] X. Tao *et al*, "Crystalline destruction caused by water tree growth in low-density polyethylene," IEEE Trans. Dielectr. Electr. Insul., vol. 28, no. 1, pp. 167–174, 2021.
[10] A. Bulinski, S. Bamji and J. Densley, "Water treeing in binary linear polyethylene blends," IEEE Trans. Dielectr. Electr. Insul., vol. 1, no. 6, pp. 949–962, 1994.
[11] Z. Fan and N. Yoshimura, "The influence of crystalline morphology on the growth of water trees in PE," IEEE Trans. Dielectr. Electr. Insul., vol. 3, no. 6, pp. 849–858, 1996.
[12] K. Li, K. Zhou and G. Zhu, "Toward understanding the relationship between the microstructure and propagation behavior of water trees," IEEE Trans. Dielectr. Electr. Insul., vol. 26, no. 4, pp. 1116–1124, 2019.
[13] I. Radu *et al*, "The effect of water treeing on the electric field distribution of XLPE consequences for the dielectric strength," IEEE Trans. Dielectr. Electr. Insul., vol. 7, no. 6, pp. 860–868, 2000.
[14] J. J. De Bellet *et al*, "Some aspects of the relationship between water treeing, morphology, and microstructure of polymers," IEEE Trans. Electr. Insul., vol. EI-22, no. 2, pp. 211–217, 1987.
[15] Alexander L E, *X-Ray diffraction methods in polymer science*, New York: Wiley Inter-science, 1969.
[16] J. J. Gilman and W. G. Johnston, "Observations of dislocation glide and climb in lithium fluoride crystals," J. Appl. Phys., vol. 27, no. 9, pp. 1018–1022, 1956.
[17] M. J. Whelan *et al*, "Dislocations and stacking faults in stainless steel," Proc. Roy. Soc. London, vol. 240, no. 1223, pp. 524–538, 1957.
[18] D. Hull, *Introduction to Dislocations*, 3rd Edition, 1984.
[19] J. Li *et al*, "The effect of accelerated water tree ageing on the properties of XLPE cable insulation," IEEE Trans. Dielectr. Electr. Insul., vol. 18, no. 5, pp. 1562–1569, 2011.
[20] S. Alapati and M. J. Thomas, "Influence of nano-fillers on electrical treeing in epoxy insulation," Sci. Meas. Tech., IET, vol. 6, pp. 21–28, 2012.
[21] I. Radu *et al*, "The effect of water treeing on the electric field distribution of XLPE consequences for the dielectric strength," IEEE Trans. Dielectr. Electr. Insul., vol. 7, no. 6, pp. 860–868, 2000.

Kangle Li was born in Pingliang, Gansu, China, in 1990. He received his B.Sc. degree in electrical engineering in 2012, M.Sc. Degree and Ph.D degree in electric power system and its Automation in 2017 and 2021, respectively, from the College of Electrical Engineering, Sichuan University, Chengdu, China. Currently, he is a lecturer in high voltage and insulation technology at the College of Electrical Engineering and Information Engineering, Lanzhou University of Technology, China. His research interests are in the aging mechanism and the fault diagnosis of solid dielectrics. He has published three papers in the IEEE *Transactions* and other journals.